

Complementarity of the CERN Large Hadron Collider and the e^+e^- International Linear Collider^{*}

S. Y. Choi^a

Department of Physics and RIPC, Chonbuk National University, Jeonju 561-756, Korea

October 30, 2018

Abstract. The next-generation high-energy facilities, the CERN Large Hadron Collider (LHC) and the prospective e^+e^- International Linear Collider (ILC), are expected to unravel new structures of matter and forces from the electroweak scale to the TeV scale. In this report we review the complementary role of LHC and ILC in drawing a comprehensive and high-precision picture of the mechanism breaking the electroweak symmetries and generating mass, and the unification of forces in the frame of supersymmetry.

PACS. 12.60.-i Models beyond the standard model – 12.60.Jv Supersymmetric models

1 Introduction

Particle physics has been very successful in unraveling the basic laws of nature at the smallest accessible length scale, and it has revealed a consistent picture, the Standard Model (SM), adequately describing the structure of matter and forces, although the elusive Higgs boson is yet to be identified [2]. However, many theoretical arguments and experimental observations indicate that the model is incomplete and that it should be embedded in a more fundamental theory, addressing a set of crucial questions to be approached experimentally at the TeV scale (Terascale): the mechanism of electroweak symmetry breaking (EWSB) and mass generation; the unification of forces, including gravity finally; and the structure of spacetime at short distances. This set of questions in particle physics is intriguingly connected to cosmology questions such as the nature of particles comprising cold dark matter (CDM) and the origin of the baryon asymmetry in the universe.

The next generation of high-energy accelerators will get access to the Terascale with high expectation of providing decisive answers to these questions [3,4]. LHC with a c.m. energy of 14 TeV [5,6] will put the first springboard in 2008 for breakthrough discoveries in the EWSB sector and in physics beyond the SM (BSM). However, the analysis of new physics processes at LHC is complicated. Therefore, an e^+e^- facility with clean environments (and, potentially, with various options such as γe and $\gamma\gamma$ collision modes and the GigaZ mode

running at an energy on top of the Z-boson resonance) is required to complement this hadron machine in drawing a comprehensive and high-resolution picture of EWSB and of the BSM. The ILC [7,8,9,10,11,12], which is now in the design phase, would be an excellent counterpart to LHC. The ILC energy of 500 GeV in the first phase and 1 TeV in the upgraded phase in the lepton sector is equivalent in many aspects to the higher LHC energy of about 5 TeV in the quark sector. Moreover, ILC covers one of the most crucial energy ranges including the characteristic EWSB scale $v = 246$ GeV. [If the BSM scale revealed at LHC might be beyond the reach of ILC, it could be accessed later by the 3-5 TeV Compact Linear Collider (CLIC) [13].]

Several dedicated studies of the interplay between LHC and ILC have been carried out [11,14,15] in the recent past. In particular, the LHC/ILC Study Group, formed as a collaborative effort of the hadron and lepton collider experimental communities and theorists, has completed a comprehensive working group report with detailed studies of various conceivable BSM scenarios [14]. Our report will not cover all these topics but it should give a concise review of the complementary role of LHC and ILC in drawing a model-independent and high-resolution picture of the new Terascale physics which may reveal the fundamental theory at scales close to the grand unification (GUT) or Planck scale. Supersymmetry (SUSY) will exclusively be considered as a BSM prototype concept in this description.

2 The supersymmetry path

In supersymmetric theories a light Higgs boson is generated and the electroweak (EW) scale is stabilized naturally in the GUT/Planck-scale background. The

^{*} Extended version of Ref.[1] to be published in “Supersymmetry on the Eve of the LHC”, a special volume of European Physical Journal C, Particles and Fields (EPJC) in memory of Julius Wess.

^a Email: sychoi@chonbuk.ac.kr

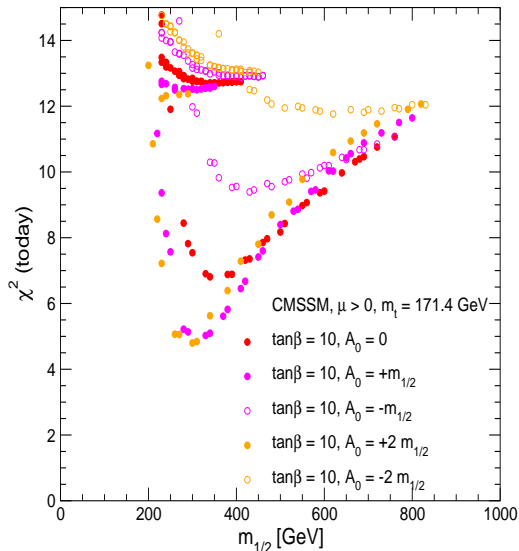


Fig. 1. The combined χ^2 function for electroweak precision observables and B -physics observables as a function of the universal gaugino mass $m_{1/2}$; Ref. [25].

presence of the supersymmetric particle spectrum is essential for the unification of the three SM gauge couplings at high energies [16,17,18,19]. It offers a natural CDM candidate. Moreover, local SUSY provides a rationale for gravity by demanding the existence of massless spin-2 gravitons. In short, if realized in nature, SUSY will have an impact across all microscopic and cosmological scales.

There is no firm prediction for the SUSY mass scale. However, direct bounds on the mass scale due to the absence of sparticles at LEP and the Tevatron have been established, and important indirect constraints from the LEP lower limit of 114 GeV on the Higgs mass [20], the observation of photonic b -decays, $b \rightarrow s\gamma$ [21,22], the BNL measurement of the anomalous magnetic moment of the muon a_μ [23], and also from the measurement of the CDM density at WMAP [24] have been derived. As shown in Fig. 1, a global fit to precision EW and B -decay observables indicates a fairly low mass-spectrum for moderate values of the Higgs mixing parameter $\tan\beta$ in minimal supergravity (mSUGRA) [25]. In this favorable case several non-colored supersymmetric particles such as lighter neutralinos and sleptons should be observed at ILC in the first phase with 500 GeV c.m. energy and even the heavier non-colored particles and the lighter top squark in the upgraded phase with the c.m. energy of 1 TeV. The spectrum corresponding to a parameter set with close to maximal probability is depicted in Fig. 2. This spectrum had been chosen as a benchmark set for an mSUGRA scenario in the SPS1a' project [26].

LHC and ILC can provide us with a perfectly combined tool for exploring SUSY [14]. The heavy colored supersymmetric particles, squarks and gluinos, can be discovered for masses up to 3 TeV with large rates at LHC. The properties of the potentially lighter non-colored particles, charginos, neutralinos, sleptons and Higgs bosons, can be studied very precisely at ILC

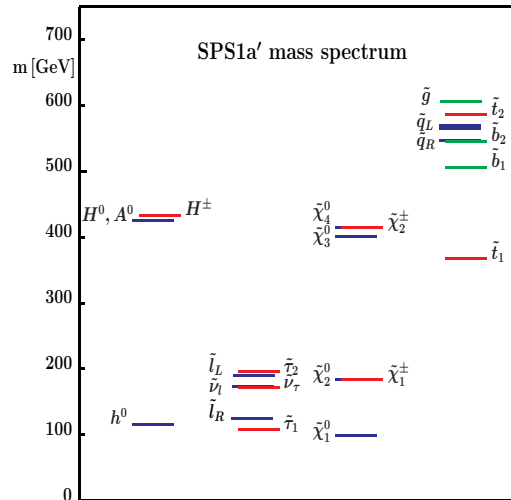


Fig. 2. Mass spectrum of supersymmetric particles and Higgs bosons in the reference point SPS1a'; Ref. [26].

by exploiting, in particular, beam polarizations [27]. Once the properties of the light particles are determined precisely at ILC, the heavier particles produced at LHC can subsequently be studied in the cascade decays with much greater precision. Based on the coherent LHC and ILC analyses we can then take the supersymmetry path by

- measuring the masses and mixings of the newly produced particles, their decay widths and branching ratios, their production cross sections, etc;
- verifying that there are indeed the superpartners of the SM particles by determining their spin and parity, gauge quantum numbers and their couplings;
- reconstructing the low energy Lagrangian with the smallest number of assumptions, i.e. as model independently as possible;
- and unraveling the fundamental SUSY breaking mechanism and shedding light on the physics at the very high energy (GUT or Planck) scale,

from the EW scale to the GUT/Planck scale – on one side, for the reconstruction of the fundamental SUSY theory near the Planck scale and, on the other side, for the connection of particle physics with cosmology.

3 Higgs bosons

In SUSY theories the Higgs sector includes at least two iso-doublet scalar fields so that at least five more physical particles are predicted [28]. In the minimal supersymmetric SM (MSSM) the mass of the lightest neutral scalar Higgs particle h is bounded from above to about 140 GeV, while the masses of the heavy neutral scalar and pseudoscalar Higgs bosons, H and A , and the charged Higgs bosons, H^\pm , may range from the EW scale to the multi-TeV scale. The upper bound on the lightest Higgs mass is relaxed only up to about 200 GeV in more general scenarios provided the fields remain weakly interacting up to the Planck scale [29].

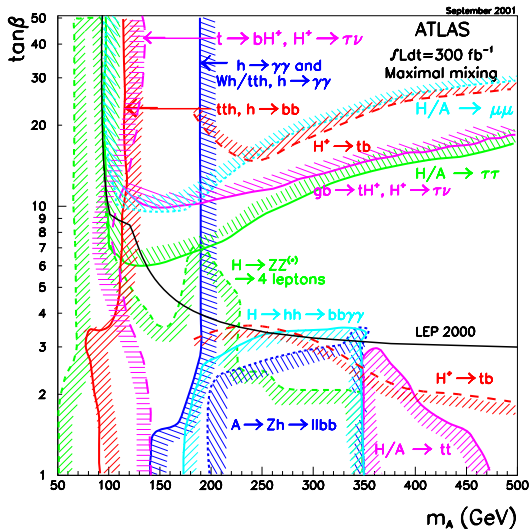


Fig. 3. The ATLAS sensitivity for the discovery of the MSSM Higgs bosons in the case of maximal mixing. The 5σ discovery curves are shown in the $(\tan\beta, m_A)$ plane for the individual channels and for an integrated luminosity of 300 fb^{-1} . The corresponding LEP limit is also shown; Ref. [30].

3.1 The MSSM Higgs Bosons

While the light Higgs boson h can be detected at LHC in the full range of the M_A and $\tan\beta$ parameter space, none of the heavy Higgs bosons can be detected in a blind wedge centered around the medium mixing angle $\tan\beta \sim 7$ and opening from masses of about 200 GeV to higher values, cf. Fig. 3 [30,31]. This region can be covered by ILC and CLIC up to the multi-TeV range.

At ILC the search and study of the light Higgs boson h follows the pattern very similar to the SM Higgs boson in most of the parameter space and the heavy Higgs bosons are produced in mixed pairs at ILC: $e^+e^- \rightarrow HA$ and H^+H^- . Therefore, the wedge can be covered by pair production in e^+e^- collisions for masses $M_{H,A} \leq \sqrt{s}/2$, i.e., up to 500 GeV in the TeV phase of the ILC machine, cf. Fig. 4 [32] and, further, up to 2.5 TeV at the 5 TeV CLIC [13]. Moreover, single production in photon-photon collisions, $\gamma\gamma \rightarrow H$ and A , can cover the wedge up to Higgs masses of 800 GeV if a fraction of 80% of the total energy of the 1 TeV ILC is transferred to the $\gamma\gamma$ system by Compton back-scattering of laser light [33]. The mass reach for the heavy Higgs bosons in $\gamma\gamma$ collisions can further be extended to 4 TeV at the 5 TeV CLIC [34].

After the Higgs bosons are discovered, it must experimentally be established that the Higgs mechanism is responsible indeed for breaking the EW symmetry and for generating the masses of the fundamental SM particles. This requires the precise profiling of the properties of the Higgs bosons. First model-independent analyses of the properties can be performed at LHC by measuring the Higgs masses, the Higgs spin(s) [35,36], the ratios of some Higgs couplings and the bounds on couplings [37].

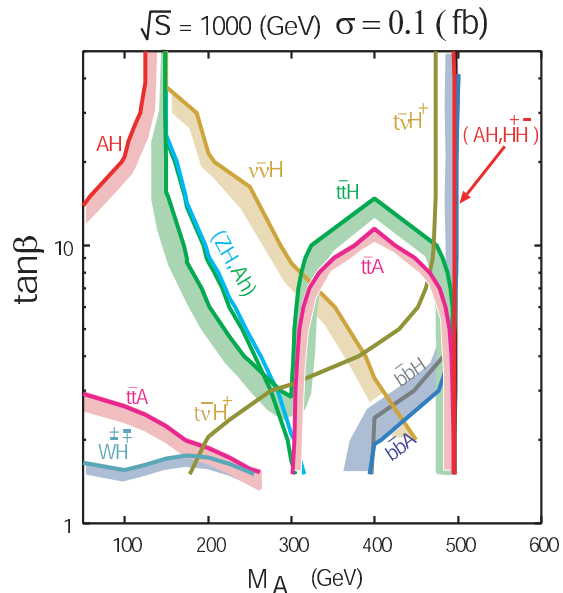


Fig. 4. Cross section contours of various heavy MSSM Higgs production processes in the $M_A/\tan\beta$ plane for $\sqrt{s} = 1 \text{ TeV}$; Ref. [32].

Coupling-Mass Relation

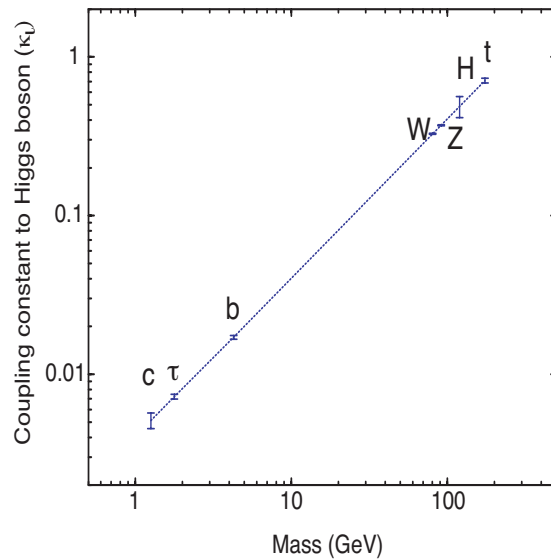


Fig. 5. The relation between the Higgs coupling of a particle and its mass in the SM. The error bars correspond to the accuracy expected from ILC data; Ref. [39].

However, the truly model-independent and high-resolution determination of the profile of the light Higgs boson h – the mass, the spin of the particle, the absolute values of the Higgs couplings to the SM particles and the trilinear Higgs self couplings – can be carried out at ILC, with clear signals of Higgs events above small backgrounds in the processes of Higgs-strahlung, $e^+e^- \rightarrow Zh$, and WW fusion, $e^+e^- \rightarrow \bar{\nu}\nu h$, and in the process of double Higgs production, $e^+e^- \rightarrow Zhh$ and $\bar{\nu}\nu hh$ [38]. As shown in Fig. 5 for typical SM particle species, the linear relation between

the Higgs couplings and the masses for typical SM particle species can be tested with great precision at ILC [39].

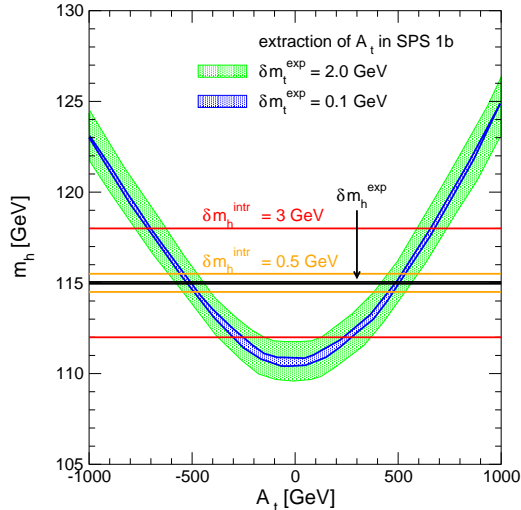


Fig. 6. Extracting the trilinear coupling A_t from radiative corrections to the light MSSM Higgs mass; Ref. [40].

High-precision measurements of the lightest Higgs mass at ILC can be exploited to determine parameters in the SUSY theory which are difficult to measure directly. For instance, by evaluating quantum corrections, the top quark trilinear coupling A_t can be calculated from the Higgs mass, Fig. 6. For an error on the top quark mass of $\delta m_t = 100$ MeV and an error on the Higgs mass of $\delta m_h = 50$ MeV, A_t can be determined at an accuracy of about 10% [40].

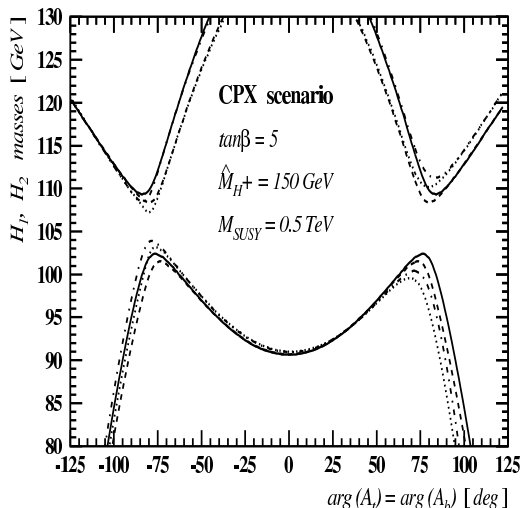


Fig. 7. Numerical estimates of the $H_{1,2}$ pole masses as a function of the CP-violating phase of the stop/sbottom trilinear parameter $A_{t,b}$; Ref. [47].

3.2 CP violation in the MSSM Higgs sector

In the general MSSM [41], the gaugino mass parameters M_i ($i = 1, 2, 3$), the higgsino mass parameter μ , and the trilinear couplings A_f can be complex so that they can induce explicit CP violation in various ways in the model. Their physical combinations affect sparticle masses and couplings through mixing, induce CP-violating mixing in the Higgs sector through radiative corrections, influence CP-even observables such as cross sections and also lead to interesting CP-odd asymmetries at colliders. As a result, although stringently constrained by low energy observables like electric dipole moments (EDMs), the nontrivial CP phases can significantly influence the collider phenomenology of Higgs and SUSY particles and also the properties of neutralino CDM [42, 43, 44].

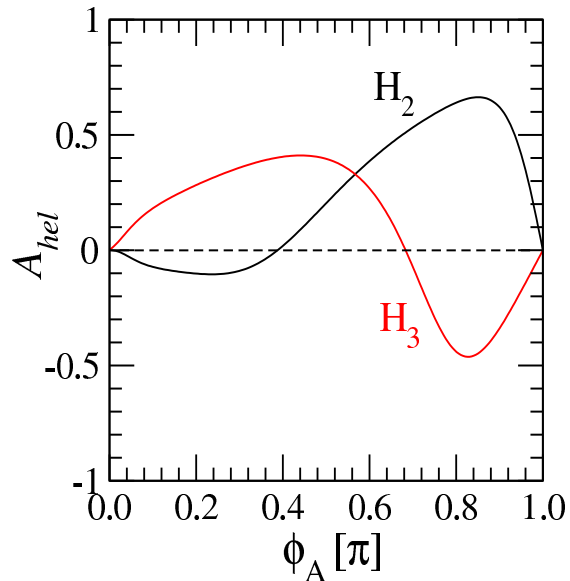


Fig. 8. The CP-odd asymmetry A_{hel} at the pole of the heavy Higgs bosons H_2 and H_3 as a function of the phase ϕ_A of the stop trilinear parameter A_t ; Ref. [46].

Referring to the CPNSH report [42] for an extensive discussion of CP violation in supersymmetric theories, we mention in this report just two examples of CP-violation in the Higgs-sector. The lightest Higgs boson H_1 without definite CP-parity may couple very weakly to the gauge bosons so that the state could have escaped detection at LEP2 [45], and the heavy Higgs states H and A can exhibit CP-violating resonant mixing phenomena when two states are degenerate in mass in the decoupling regime [46]. One example of the impact of the CP-violating Higgs mixing on the Higgs mass spectrum is shown in Fig. 7 as a function of the phase of the stop and sbottom trilinear coupling $A_{t,b}$ [47]. The other example for studying the CP-violating resonant mixing of two heavy neutral Higgs bosons is provided by $\gamma\gamma$ -Higgs formation in polarized beams. As shown in Fig. 8, the CP violation due to resonant H/A mixing can directly be probed via the CP-odd

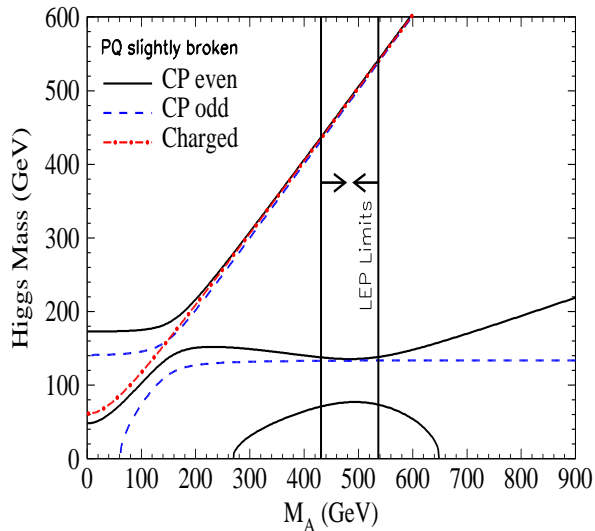


Fig. 9. Typical Higgs mass spectrum in the NMSSM; Ref [48].

asymmetry $A_{hel} = (\sigma_{++} - \sigma_{--})/(\sigma_{++} + \sigma_{--})$ constructed with circular photon polarization [46].

3.3 Extended Higgs sector

A large variety of BSM theories such as GUT theories and string theories suggest extended gauge and Higgs sectors with additional gauge bosons and Higgs bosons beyond the minimal set of the MSSM [48, 49, 50, 51, 52, 53].

The next-to-MSSM (NMSSM), the simplest extension of the MSSM, introduces a complex iso-scalar field, generating a weak scale higgsino mass parameter μ by spontaneous symmetry breaking in the Higgs sector. The NMSSM Higgs sector is thus extended to include an additional scalar and a pseudoscalar. The axion-type character of the pseudoscalar boson renders this particle preferentially light. An example for the mass spectrum [48] is shown in Fig. 9. Since the trilinear couplings increase with energy, upper bounds on the mass of the lightest neutral scalar Higgs boson can be derived from the assumption that the theory be valid up to the GUT scale: $m(H_1) \lesssim 140$ GeV. Thus, in spite of the additional interactions, the distinct pattern of the minimal extension remains valid also in more complex supersymmetric scenarios. If H_1 is (nearly) pure isosinglet, the coupling ZZH_1 is small and the particle cannot be produced by Higgs-strahlung. However, in this case H_2 is generally light and couples with sufficient strength to the Z boson; if not, H_3 plays this role, so that one Higgs boson can be discovered in any case.

A large variety of other extensions beyond the SM has been analyzed theoretically. For instance, if the gauge boson sector is expanded by an additional $U(1)'$

Abelian symmetry at high energies [52], the additional pseudoscalar Higgs field is absorbed to generate the mass of the new Z' boson while the scalar part of the Higgs field can be observed as a new Higgs boson beyond the MSSM set. If generated by an extended symmetry like E_6 , the Higgs sector is expanded by an ensemble of new states [53] with quite unconventional properties.

Quite generally, as long as the fields in supersymmetric theories remain weakly interacting up to the canonical Planck scale, the mass of the lightest Higgs bosons is bounded to about 200 GeV as the Yukawa couplings are restricted to be small in the same way as the quartic coupling in the standard Higgs potential. Moreover, the mass bound of 140 GeV for the lightest Higgs particle is realized in almost all supersymmetric theories [54]. Consequently, experiments at ILC with 500 GeV c.m. energy are in a *no-lose* situation [55] for detecting the Higgs particles even in general supersymmetric theories.

4 Supersymmetric particles

For an explicit numerical illustration we adopt the parameters of the minimal supergravity reference point SPS1a' [26]. It is characterized by the following values of the soft parameters at the GUT scale: $M_{1/2} = 250$ GeV, $M_0 = 70$ GeV, $A_0 = -300$ GeV, $\text{sign}(\mu) = +$ and $\tan\beta = 10$ where $M_{1/2}$, M_0 , A_0 and μ denote the universal gaugino mass, the universal scalar mass, the universal trilinear coupling and the higgsino mass parameter. The modulus of the higgsino mass parameter is fixed by requiring radiative electroweak symmetry breaking [56, 57, 58, 59, 60] so that $\mu = +396$ GeV. As shown by the sparticle and Higgs spectrum in Fig. 2, the squarks and gluinos can be studied very well at LHC and the non-colored charginos and neutralinos, sleptons and Higgs bosons can be analyzed partly at LHC and studied precisely at ILC operating at a c.m. energy up to 1 TeV.

4.1 Masses of supersymmetric particles

At LHC, the masses can be obtained by analyzing edge effects in the cascade decay spectra, cf. Ref. [61]. An ideal chain is a long sequence of two-body decays: $\tilde{q}_L \rightarrow \tilde{\chi}_2^0 q \rightarrow \tilde{\ell}_R \ell q \rightarrow \tilde{\chi}_1^0 \ell \ell q$. The kinematic edges and thresholds predicted in the invariant mass distributions of the two leptons and the jet determine the masses in a model-independent way [61]. The four particle masses measured by this method are used subsequently as input for other decay chains like $\tilde{g} \rightarrow \tilde{b}_1 b \rightarrow \tilde{\chi}_2^0 b b$ and the shorter chains $\tilde{q}_R \rightarrow q \tilde{\chi}_1^0$ and $\tilde{\chi}_4^0 \rightarrow \tilde{\ell} \ell$. However, there are residual ambiguities and the strong correlations between the heavier masses and the lightest supersymmetric particle (LSP).

At ILC very precise mass values can be extracted from threshold scans and decay spectra [62]. The excitation curves for chargino $\tilde{\chi}_{1,2}^\pm$ production in S-waves

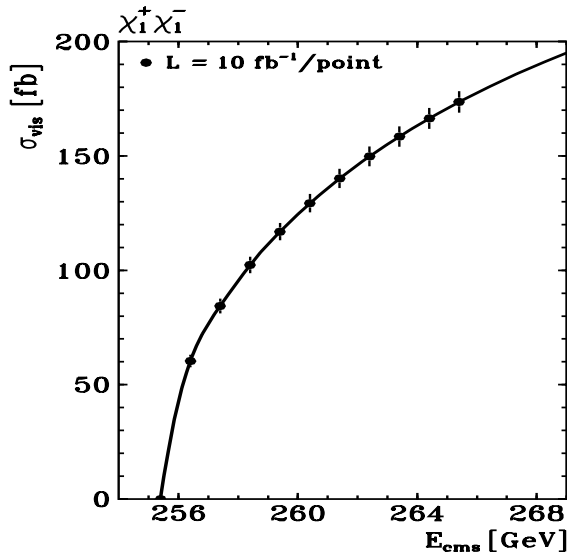


Fig. 10. Mass measurement at the threshold of chargino $\tilde{\chi}_1^+ \tilde{\chi}_1^-$ pair production; Ref [62].

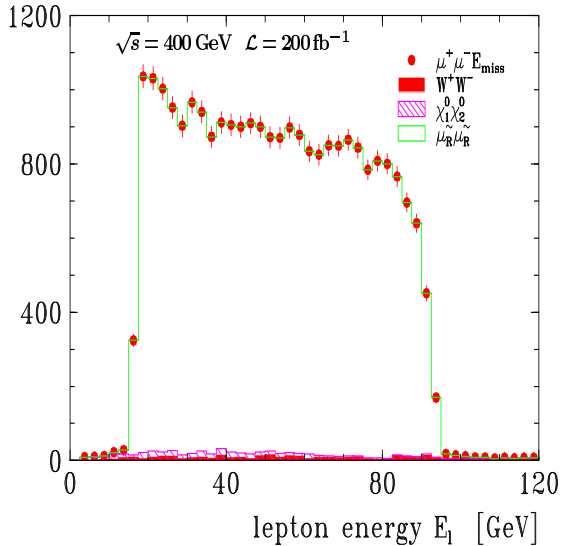


Fig. 11. Smuon and neutralino edges in two-body smuon decays, $\tilde{\mu}_R^\pm \rightarrow \mu^\pm \tilde{\chi}_1^0$; Ref [62].

rise steeply with the velocity of the particles near threshold and they are thus very sensitive to the mass values, cf. Fig. 10. The same holds true for mixed chiral selectron pairs in $e^+e^- \rightarrow \tilde{e}_R^+ \tilde{e}_L^-$ and for diagonal pairs in $e^-e^- \rightarrow \tilde{e}_R^- \tilde{e}_R^-, \tilde{e}_L^- \tilde{e}_L^-$ [63,64]. Other scalar fermions as well as neutralinos are produced in P-waves with a less steep threshold behavior proportional to the third power of the velocity. Important information on the mass of the LSP such as the lightest neutralino $\tilde{\chi}_1^0$ can be obtained from the sharp edges of two-body decay spectra as $\tilde{\ell}_R \rightarrow \ell \tilde{\chi}_1^0$, cf. Fig. 11 [62]. The accuracy in the measurement of the LSP mass can be improved at ILC by two orders of magnitude compared with LHC; Tab. 1.

The values of typical mass parameters and their related measurement errors are presented in Tab. 1: “LHC” from LHC analyses and “ILC” from ILC anal-

Table 1. Accuracies of representative mass measurements of SUSY particles in individual LHC, ILC and coherent LHC/ILC analyses in the point SPS1a’ [mass units in GeV]; Ref. [26].

Particles	Mass	“LHC”	“ILC”	“LHC+ILC”
h^0	116.0	0.25	0.05	0.05
H^0	425.0		1.5	1.5
$\tilde{\chi}_1^0$	97.7	4.8	0.05	0.05
$\tilde{\chi}_2^0$	183.9	4.7	1.2	0.08
$\tilde{\chi}_4^0$	413.9	5.1	3-5	2.5
$\tilde{\chi}_1^\pm$	183.7		0.55	0.55
\tilde{e}_R	125.3	4.8	0.05	0.05
\tilde{e}_L	189.9	5.0	0.18	0.18
$\tilde{\tau}_1$	107.9	5-8	0.24	0.24
\tilde{q}_R	547.2	7-12	-	5-11
\tilde{q}_L	564.7	8.7	-	4.9
\tilde{t}_1	366.5		1.9	1.9
\tilde{b}_1	506.3	7.5	-	5.7
\tilde{g}	607.1	8.0	-	6.5

yses. The fourth column “LHC+ILC” represents the corresponding errors if the experimental analyses are performed coherently [26].

4.2 Spins of supersymmetric particles

Determining the spin of new particles is an important method to clarify the nature of the particles and the underlying theory. This determination is crucial to distinguish the supersymmetric interpretation of new particles from other models.

The measurement of the spins in particle cascades at LHC is quite involved [65,66,67]. While the invariant mass distributions of the particles in decay cascades are characteristic for the spins of the intermediate particles involved, detector effects strongly reduce the signal in practice.

In contrast, the spin measurement at ILC is straightforward [68,69]. Even though the P-wave onset of the excitation curve is a necessary but not sufficient condition, the $\sin^2 \theta$ law for the angular distribution in the production of sleptons (for selectrons close to threshold) is a unique signature of the fundamental spin-zero character; Fig. 12. On the contrary, neither the onset of the excitation curves near threshold nor the angular distribution in the production processes provide unique signals of the spin of charginos and neutralinos. However, decay angular distributions of polarized charginos/neutralinos, as generated naturally in e^+e^- collisions, can provide an unambiguous determination of the spin-1/2 character of the particles albeit at the expense of more involved experimental analyses [69]. [Quantum interference among helicity amplitudes, reflected in azimuthal angle distributions, may provide another method for determining spins [70]. However, this method depends strongly on the masses of the decay products and the c.m. energy, as the quantum interference disappears with increasing energy.]

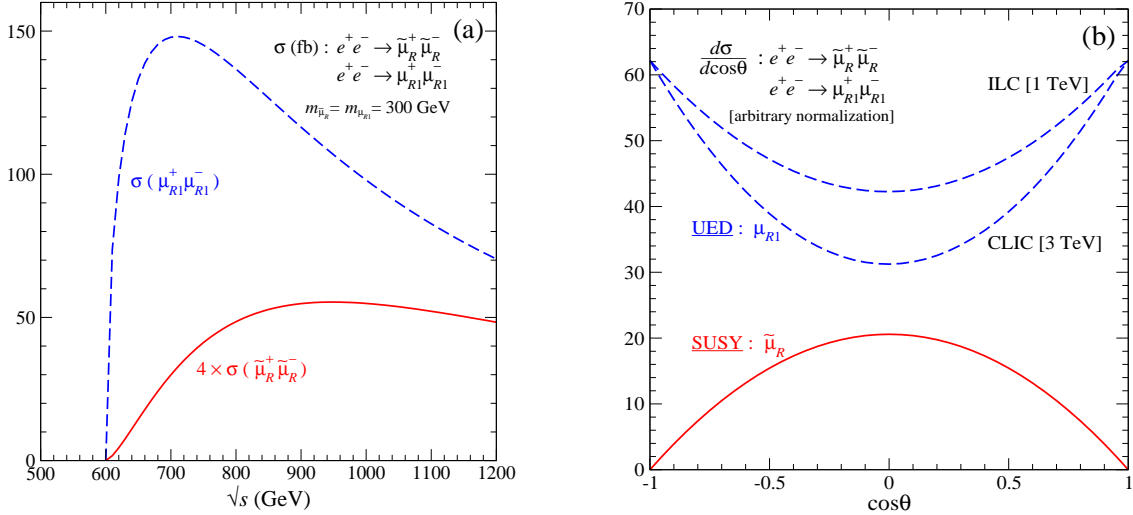


Fig. 12. The threshold excitation (a) and the angular distribution (b) in the case of smuons in the MSSM, compared with the first spin-1/2 Kaluza-Klein muons in a model of universal extra dimensions, in pair production at ILC; for details, see Ref. [69].

4.3 Mixings of supersymmetric particle states

Mixing parameters must be extracted from measurements of cross sections and polarization asymmetries. [The determinations of mixing parameters are difficult at LHC since several production and decay processes are simultaneously involved and only the products of the production cross sections and the decay branching fractions are measured experimentally.] In the production of charginos and neutralinos, both diagonal and non-diagonal pairs can be exploited: $e^+e^- \rightarrow \tilde{\chi}_i^+ \tilde{\chi}_j^-$ [$i, j = 1, 2$] [71,72,73] and $\tilde{\chi}_i^0 \tilde{\chi}_j^0$ [$i, j = 1, \dots, 4$] [74]. The production cross sections for charginos are binomials in $\cos 2\phi_{L,R}$ where $\phi_{L,R}$ are the mixing angles rotating current to mass eigenstates. Using polarized electron and positron beams, the mixings can be determined in a model-independent way, Fig. 13. The same procedures can be applied to determine the mixings in the sfermion sector [75,76,77,78]. The production cross sections for stop particle pairs, $e^+e^- \rightarrow \tilde{t}_i \tilde{t}_j^*$ [$i, j = 1, 2$], depend on the stop mixing angle $\theta_{\tilde{t}}$ which can be determined with high accuracy by use of polarized electron beams [77,78].

4.4 Supersymmetric Yukawa couplings

SUSY predicts the identity of Yukawa and gauge couplings among supersymmetric partners for gauge bosons and gauginos, and for fermions and their scalar partners.

The identity of the SU(3) QCD Yukawa and gauge couplings can be studied experimentally at LHC through pair production of squarks partly mediated by gluino t -channel exchanges [79,80]. A potential complement [81] to this method is gluino emission in association with quark-squark final states in e^+e^- collisions, $e^+e^- \rightarrow q\tilde{q}\tilde{g}$, which might be kinematically accessible at the second phase of ILC and/or at CLIC. While the $q\tilde{q}\tilde{g}$

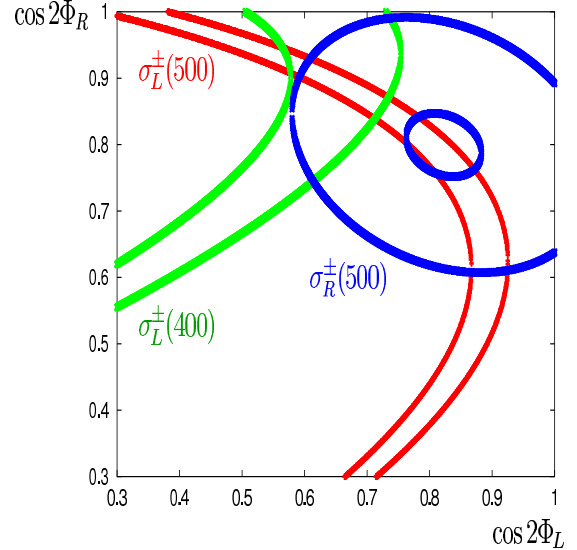


Fig. 13. Contours of mixing angles for the $e^+e^- \rightarrow \tilde{\chi}_1^+ \tilde{\chi}_1^-$ production cross section for polarized e^\pm beams at $\sqrt{s} = 400$ and 500 GeV; Ref. [73].

channel measures the $q\tilde{q}\tilde{g}$ Yukawa coupling, the radiation processes $\tilde{q}\tilde{q}g$ and qqg determine the QCD gauge coupling in the squark sector and the standard quark sector for comparison.

On the other hand the SU(2) weak and U(1) hypercharge relations can be confirmed experimentally at ILC through pair production of charginos and neutralinos which is partly mediated by the exchange of sneutrinos and selectrons in the t -channel [74], as well as selectron and sneutrino production which is partly mediated by neutralino and chargino exchanges [64]. The separation of the electroweak SU(2) and U(1) couplings is also possible if polarized electron beams are available. Of course the analysis for confirming the identity of Yukawa and gauge couplings should be performed by taking into account the prior measurements

of the masses and/or mixing parameters of the particles exchanged in the t -channel. Taking into account uncertainties from the selectron and the neutralino parameters, the SU(2) and U(1) Yukawa couplings can be extracted with a precision of 0.7% and 0.2%, respectively, at ILC with a 500 GeV energy and 500 fb^{-1} integrated luminosity in the SPS1a' scenario.

4.5 Majorana versus Dirac fermions

The parallelism between self-conjugate neutral vector gauge bosons and their fermionic supersymmetric partners induces the Majorana nature of these particles in the minimal formulation of the theory. Nevertheless, experimental tests of the Majorana character of gluinos and neutralinos would provide non-trivial insight into the realization of SUSY in nature, since extended supersymmetric models can include Dirac gauginos. $N = 2$ SUSY provides a solid theoretical basis for formulating such a testing ground [82]. Since the fermionic degrees of freedom are doubled in the gauge sector, the ensuing two Majorana fields can be joined to a single Dirac field if the masses are chosen identical.

There are several methods to investigate the Majorana nature of gluinos at LHC. In the original form, decays to heavy stop/top quarks are exploited [83] to test whether the final state in the fermion decay $\tilde{g} \rightarrow \tilde{t}\tilde{t} + \tilde{t}^*t$ is self-conjugate. The standard production processes for investigating the Majorana nature of gluinos [84] are the production of a pair of equal-chirality squarks, $q_L q_L \rightarrow \tilde{q}_L \tilde{q}_L$ and $q_R q_R \rightarrow \tilde{q}_R \tilde{q}_R$. While the cross section for the scattering processes with equal-chirality quarks is non-zero in the Majorana theory, it vanishes in the Dirac theory. Owing to the dominance of u -quarks over d -quarks in the proton, the Majorana theory predicts large rates of like-sign dilepton final states from squark pair production with an excess of positively charged leptons while they are absent, apart from a small number of remnant channels, in the Dirac theory. [In a realistic analysis one has to include gluino production processes which can also feed the like-sign dilepton signal but can be discriminated by extra jet emission from the gluino decays.]

On the other hand, the Majorana/Dirac nature of neutralinos can be studied through very clean reactions, $e^-e^- \rightarrow \tilde{e}^-\tilde{e}^-$, in the e^-e^- collision mode of ILC with left/right-handedly polarized beams [84, 85, 86].

4.6 Split supersymmetry

For the unification of forces at the GUT scale the sfermion mass scale M_0 is irrelevant, since each generation of sfermions furnishes a complete SU(5) [or SO(10), if right-handed sneutrinos are included]. Likewise, the dark-matter prediction of the MSSM and its extensions does not rely on the value of M_0 , but rather on the existence of a conserved discrete quantum number, R-parity. These quantitative considerations led to

the speculation that the sfermion mass scale may actually be much higher than the gaugino mass scale, effectively removing all scalar partners of the matter fields and the extra heavy Higgs states of the MSSM from the low-energy spectrum [87].

With such a high sfermion mass scale, e.g., $M_0 \sim 10^9 \text{ GeV}$, the gluino acquires a macroscopic lifetime and, for the purpose of collider experiments, it behaves like a massive, stable color-octet parton. This leads to characteristic signatures at LHC. However, due to the absence of cascade decays, the production of the non-colored gauginos and higgsinos at LHC proceeds only via EW annihilation processes, and the production rates are thus considerably suppressed compared to conventional MSSM scenarios.

In this situation, the analysis of chargino and neutralino pair-production at ILC provides the information necessary to deduce the supersymmetric nature of the model [88]. Extracting the values of chargino and neutralino Yukawa couplings, responsible for the mixing of gaugino and higgsino states, reveals the anomalous effects due to the splitting of gaugino and sfermion mass scales.

5 The fundamental theory

Combining the information from LHC on the generally heavy colored particles with the information from ILC on the generally lighter non-colored particle sector (and later from CLIC on heavier states) will generate a model-independent and high-precision picture of SUSY at the Terascale. The picture may subsequently serve as a solid platform for the reconstruction of the fundamental SUSY theory at a high scale, potentially close to the Planck scale, and for the analysis of the microscopic mechanism of SUSY breaking [89, 90]. The experimental accuracies expected at the per-cent down to the per-mil level must be matched on the theoretical side. This demands a well-defined framework for the calculational schemes in perturbation theory as well as for the input parameters like a recently proposed scheme called Supersymmetry Parameter Analysis (SPA) [26].

5.1 Linking Terascale SUSY to the GUT/Planck scale

If SPS1a' or a similar SUSY parameter set is realized in nature, various channels can be exploited to extract the basic Terascale SUSY parameters at LHC and ILC. The data analysis performed coherently for LHC and ILC gives rise to a very precise picture of the supersymmetric particle spectrum. Running global analysis programs for the whole set of data enables us to extract the Lagrangian parameters in the optimal way after including radiative corrections [91, 92, 93, 94, 95]. The present quality of such an analysis can be judged from the results shown in Tab. 2.

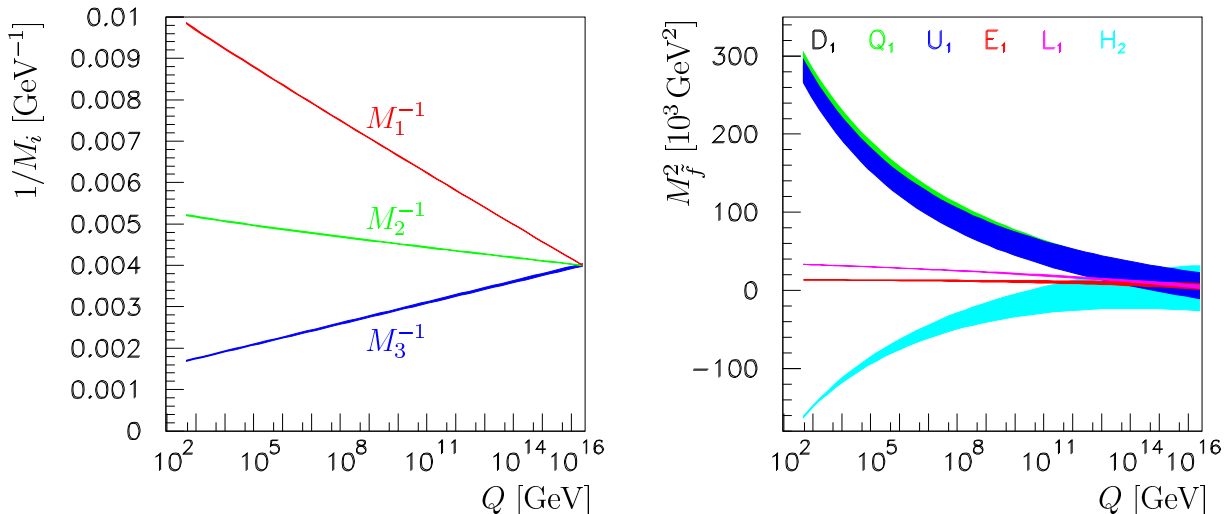


Fig. 14. The evolution of the gaugino and scalar mass parameters with the scale Q in SPS1a'. Only experimental errors are taken into account; theoretical errors are assumed to be reduced to the same size in the future; Ref. [89].

Table 2. Excerpt of extracted SUSY Lagrangian mass and Higgs parameters at the Terascale in the reference point SPS1a' [mass units in GeV]; Ref. [26].

Parameter	SPS1a' value	Fit error [exp]
M_1	103.3	0.1
M_2	193.2	0.1
M_3	571.7	7.8
μ	396.0	1.1
M_{L_1}	181.0	0.2
M_{E_1}	115.7	0.4
M_{L_3}	179.3	1.2
M_{Q_1}	525.8	5.2
M_{D_1}	505.0	17.3
M_{Q_3}	471.4	4.9
m_A	372.0	0.8
A_t	-565.1	24.6
$\tan \beta$	10.0	0.2

Based on the parameters extracted at the Terascale we can reconstruct the fundamental SUSY theory and the related microscopic picture of the SUSY breaking mechanism [89]. The experimental information is exploited to the maximum extent possible in the bottom-up approach in which the extrapolation from the Terascale to the GUT/Planck scale is performed by the renormalization group (RGE) evolution of all parameters, with the GUT scale defined by the unification point of the gauge couplings.

Typical examples for the evolution of the gaugino and scalar mass parameters are presented in Fig. 14. While the determination of the high-scale parameters in the gaugino and higgsino sector, as well as in the non-colored slepton sector, is very precise, the picture of the colored scalar and Higgs sectors is still coarse so that efforts should be made to refine it considerably. If the structure of the theory at the GUT scale were known a priori and merely the experimental determination of the high scale parameters were lacking, then

the top down-approach would lead to a very precise parametric picture at the Terascale.

So far, we have only considered the MSSM, in particular the parameter set SPS1a', as a benchmark scenario for judging the coherent capabilities of LHC and ILC experiments for the analysis of future SUSY data. However, neither this specific point nor the MSSM itself may be the correct model for low-scale SUSY. Various extended models beyond the MSSM have therefore to be investigated. The ILC experiments are crucial in discriminating between such various theories beyond the SM as they enable us to measure low-scale parameters directly with great precision and to estimate high-scale parameters reasonably well.

5.2 Left-right supersymmetric extension

A well-motivated example of model parameterizations at the very high scale, different from the mSUGRA scenario, is provided by models incorporating the right-handed neutrino sector to accommodate the complex structure observed in the neutrino sector. This requires the extension of the MSSM by a superfield including the right-handed neutrino field together with its scalar partner. If the small neutrino masses are generated by the seesaw mechanism, a similar type of spectrum is induced in the scalar sneutrino sector, splitting into light TeV scale and very heavy masses. The intermediate seesaw scales will affect the evolution of the SUSY breaking soft mass terms at the high (GUT) scale, especially in the third generation with large Yukawa couplings. This provides us with the opportunity to measure, indirectly, the intermediate seesaw scale of the third generation [96,97].

To be specific, we focus on a simple model incorporating one-step symmetry breaking from an SO(10) GUT model (with the Yukawa couplings of the neutrino sector proportional to the up-type quark mass matrix) down to the SM. Since the ν_R is unfrozen only if the RGE scale Q is beyond its mass scale $M_{\nu_R} \sim$

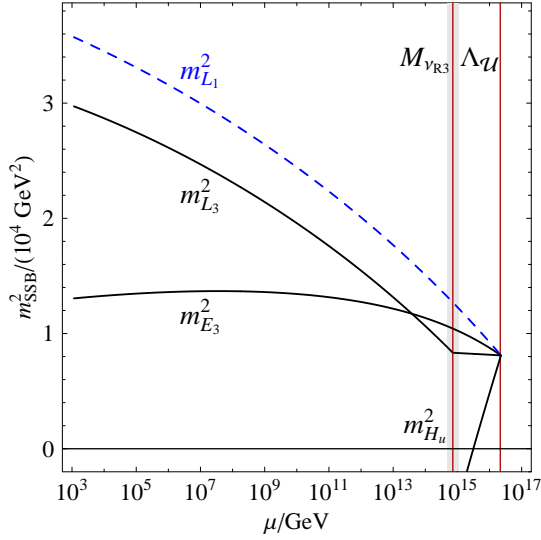


Fig. 15. Evolution of the first and third generation left- and right-handed slepton and Higgs mass parameters when loops involving the right-handed neutrino superfield are included; Ref. [97].

$m_{\tilde{L}_1}^2/m_{\nu_3} \sim 7 \times 10^{14}$ GeV the impact of the left-right extension becomes visible in the evolution of the scalar mass parameters only at very high scales. In addition, the effect of ν_R can be manifest only in the third generation where the Yukawa coupling is large. In Fig. 15 the evolution of the first and third generation left- and right-handed slepton and Higgs mass parameters are displayed. The lines include the effects of the right-handed neutrino which induce the kink in $m_{\tilde{L}_3}^2$. The kink shifts the physical masses squared of the $\tilde{\tau}_L$ and $\tilde{\nu}_{\tau_L}$ particles of the third generation by an amount Δ_{ν_τ} compared with the slepton masses of the first two generations. The precise measurement of Δ_{ν_τ} at ILC can be exploited to determine the neutrino seesaw scale of the third generation, $M_{\nu_{R3}} = 4.7$ to 11.2×10^{14} GeV.

Before closing this section, we note that other extended scenarios with CP violation, R-parity violation [98], flavor violation [99], NMSSM [100, 101] and/or extended gauge groups [53, 52] also are among the paths nature may have taken. It is, therefore, strongly recommended that the analysis conventions and methods be so general that they can be applied to all those BSM scenarios as well.

6 Dark matter and baryon asymmetry

Collider physics programs focus in connection with cosmology on two fundamental problems [102, 103]; the particle character of cold dark matter (CDM), $\rho_{\text{CDM}} = 23 \pm 4\%$, and the mechanism responsible for the baryon asymmetry, $\rho_B = 4.0 \pm 0.4\%$. These central problems cannot be solved within the framework of the SM, but various solutions have been worked out in the context of the BSM models. LHC and ILC experiments are expected to play a decisive role in clarifying the nature of CDM and in establishing the true mechanism for generating the baryon asymmetry in the universe.

6.1 Cold dark matter

Since there is no proper CDM particle candidate in the SM, the presence of CDM is a clear evidence for physics beyond the SM. In SUSY theories with R-parity the LSP is absolutely stable and represents a good CDM candidate [24]. In particular, the lightest neutralino is considered to be a prime candidate, but other interesting possibilities are the the gravitino and the axino.

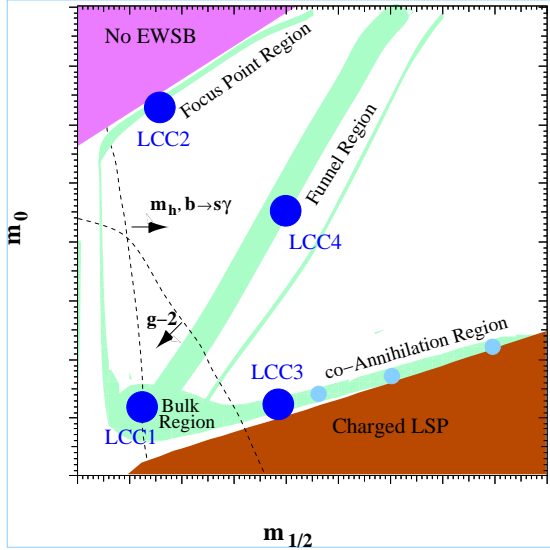


Fig. 16. The CDM-favored regions in the parameter space of the universal gaugino and sfermion mass parameters, $m_{1/2}$ and m_0 with all experimental and theoretical constraints imposed; Ref. [104, 105].

In certain areas of the SUSY parameter space with the $\tilde{\chi}_1^0$ relic density in the range required by WMAP, SUSY particles can be produced abundantly at LHC and ILC. However, to predict the WMAP relic density, we must have detailed knowledge not only of the LSP properties but also of all other particles contributing to the LSP pair annihilation cross section. To quantify the prospects for determining the neutralino CDM relic density at ILC as well as LHC, four benchmark mSUGRA scenarios called LCC points and compatible with WMAP data have been proposed, cf. Fig. 16 [105]. The ILC measurements at $\sqrt{s} = 0.5$ TeV and 1 TeV for various sparticle masses and mixings in the scenarios, taking into account LHC data, are compared to those which can be obtained using LHC data (after a qualitative identification of the model). As can be seen in Fig. 17 for two LCC points, the LCC1 “bulk” point, close to SPS1a’, and the LCC2 “focus-point” point, the gain in sensitivity by combining LHC and ILC is spectacular.

In supergravity models the gravitino \tilde{G} itself may be the LSP, building up the dominant CDM component [106, 107, 108, 109]. In such a scenario, with a gravitino mass in the range of 100 GeV, the lifetime of the next-to-LSP (NLSP) can become macroscopic as the gravitino coupling is only of gravitational strength.

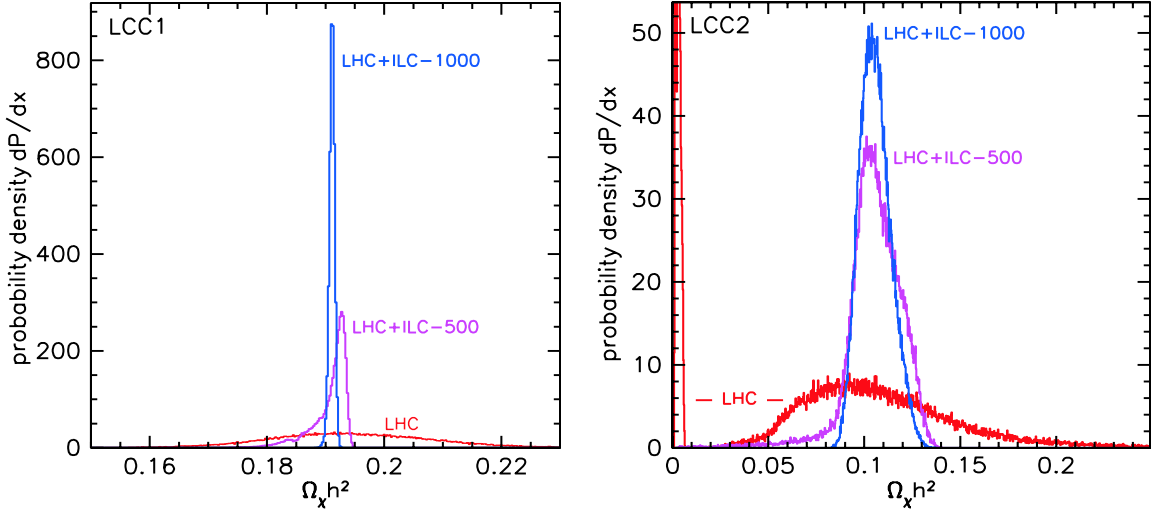


Fig. 17. Probability distribution of predictions for $\Omega_\chi h^2$ for the LCC1 [SPS1a'] “bulk” point and the LCC2 “focus-point” point from measurements at ILC with $\sqrt{s} = 0.5$ and 1 TeV, and LHC (after qualitative identification of the model); Ref. [105].

Special experimental efforts are needed to catch the long-lived $\tilde{\tau}$'s and to measure their lifetime [110,111, 112,113]. Tau slepton pair production at ILC determines the $\tilde{\tau}$ mass and the observation of the τ energy in the $\tilde{\tau}$ decay determines the gravitino mass. The measurement of the lifetime can subsequently be exploited to determine the Planck scale, a unique opportunity in a laboratory experiment.

6.2 Baryon asymmetry

Two approaches for generating the baryon asymmetry are widely discussed in the literature: baryogenesis mediated by leptogenesis and EW baryogenesis based on the supersymmetric extension of the SM.

6.2.1 Leptogenesis

If leptogenesis is the origin of the observed baryon asymmetry, the roots of this phenomenon are located near the Planck scale [114]. CP-violating decays of heavy right-handed Majorana neutrinos generate a lepton asymmetry which is transferred to the quark sector by sphaleron processes. Heavy neutrino mass scales as introduced in the seesaw mechanism for generating light neutrino masses and the size of the light neutrino masses define a self-consistent frame which is compatible with all experimental observations [115].

As shown previously, in some SUSY models the size of the heavy seesaw scales can be related to the values of the charged and neutral slepton masses. The excellent resolution of ILC in measuring the slepton masses can then be used to estimate the GUT-scale mass of the heaviest right-handed neutrino within a factor of two.

6.2.2 EW baryogenesis

One of the conditions for generating the baryon asymmetry of the universe requires the departure from thermal equilibrium. If triggered by sphaleron processes at the EW phase transition, the transition must be sufficiently strong of first order. Given the present bounds on the Higgs mass, this cannot be realized in the SM. However, since top and stop fields modify the Higgs potential strongly through radiative corrections, SUSY scenarios can give rise to first-order transitions, cf. Ref. [116]. The parameter space of the MSSM is tightly constrained in this case: The mass of the light Higgs boson is bounded by 120 GeV from above, and the mass of the light stop quark is required to be smaller than the top quark mass.

This scenario suggests that the mass of the stop quark is only slightly less than the lightest neutralino mass. The correct CDM density is generated by stop-neutralino co-annihilation in this region of parameter space, leading to tight constraints for the masses of the two particles.

While studies of the light stop quark are very difficult at hadron colliders if the main decay channel is the two-body decay $\tilde{t}_1 \rightarrow c\tilde{\chi}_1^0$ with a low-energy charm jet in the final state, the clean ILC environment allows for precision studies of the system also in such configurations [117,118].

7 Conclusions

The next generation of high energy experiments, LHC and ILC (and also CLIC later), will usher us into the Terascale, opening a new territory which is expected to generate a wealth of ground-breaking discoveries. The physics programme of both LHC and ILC in exploring this microscopic world will be very rich, with unique characteristics depending on the BSM physics

scenario realized in nature. Furthermore, as demonstrated by dedicated studies using the SUSY models, the physics potential of LHC and ILC can significantly be extended by coherent or/and “concurrent” running of both machines.

In summary, the LHC and ILC experiments with different advantages and capabilities can contribute coherently and complementarily to solutions of key questions in particle physics and cosmology. Both experiments can eventually provide us with a comprehensive and high-resolution picture not only of SUSY but also of any alternative scenario, serving as a telescope to unification scenarios of matter and interactions, and connecting particle physics and cosmology.

Acknowledgements

Special thanks go to P. M. Zerwas for the critical reading of the manuscript. This work was supported in part by the Korea Research Foundation Grant funded by the Korean Government (MOEHRD, Basic Research Promotion Fund) (KRF-2008-521-C00069) and in part by KOSEF through CHEP at Kyungpook National University.

References

1. S. Y. Choi, arXiv:0711.1393 [hep-ph].
2. C. Amsler *et al.* [Particle Data Group], Phys. Lett. B **667** (2008) 1.
3. F. Wilczek, arXiv:0708.4236 [hep-ph].
4. J. Ellis, arXiv:0710.4959 [hep-ph].
5. ATLAS TDR, CERN/LHCC/99/15.
6. CMS TDR, CERN/LHCC/2006-021.
7. H. Murayama and M. E. Peskin, Ann. Rev. Nucl. Part. Sci. **46** (1996) 533 [arXiv:hep-ex/9606003].
8. E. Accomando *et al.* [ECFA/DESY LC Physics Working Group], Phys. Rept. **299** (1998) 1 [arXiv:hep-ph/9705442].
9. K. Abe *et al.* [ACFA Linear Collider Working Group], arXiv:hep-ph/0109166.
10. T. Abe *et al.* [American Linear Collider Working Group], arXiv:hep-ex/0106055, hep-ex/0106056, hep-ex/0106057 and hep-ex/0106058.
11. J. A. Aguilar-Saavedra *et al.* [ECFA/DESY LC Physics Working Group], arXiv:hep-ph/0106315.
12. W. Kilian and P. M. Zerwas, arXiv:hep-ph/0601217.
13. E. Accomando *et al.* [CLIC Physics Working Group], arXiv:hep-ph/0412251.
14. G. Weiglein *et al.* [LHC/LC Study Group], Phys. Rept. **426** (2006) 47 [arXiv:hep-ph/0410364].
15. A. Djouadi, J. Lykken, K. Monig, Y. Okada, M. J. Oreglia and S. Yamashita, arXiv:0709.1893 [hep-ph].
16. U. Amaldi, W. de Boer and H. Furstenau, Phys. Lett. B **260** (1991) 447.
17. J. R. Ellis, S. Kelley and D. V. Nanopoulos, Phys. Lett. B **260** (1991) 131.
18. C. Giunti, C. W. Kim and U. W. Lee, Mod. Phys. Lett. A **6** (1991) 1745.
19. P. Langacker and M. x. Luo, Phys. Rev. D **44** (1991) 817.
20. J. Alcaraz *et al.* [ALEPH Collaboration], arXiv:hep-ex/0612034.
21. M. Misiak *et al.*, Phys. Rev. Lett. **98** (2007) 022002 [arXiv:hep-ph/0609232].
22. T. Becher and M. Neubert, Phys. Rev. Lett. **98** (2007) 022003 [arXiv:hep-ph/0610067].
23. S. Heinemeyer, arXiv:0710.3022 [hep-ph].
24. K. A. Olive, arXiv:0709.3303 and arXiv:0806.1208 [hep-ph].
25. J. R. Ellis, S. Heinemeyer, K. A. Olive, A. M. Weber and G. Weiglein, JHEP **0708** (2007) 083 [arXiv:0706.0652 [hep-ph]]; G. Weiglein, arXiv:0711.0200 [hep-ph].
26. J. A. Aguilar-Saavedra *et al.*, Eur. Phys. J. C **46** (2006) 43 [arXiv:hep-ph/0511344].
27. G. A. Moortgat-Pick *et al.*, Phys. Rept. **460** (2008) 131 [arXiv:hep-ph/0507011].
28. For a review, see, for example, M. Gomez-Bock, M. Mondragon, M. Muhlleitner, M. Spira and P. M. Zerwas, arXiv:0712.2419 [hep-ph].
29. J. R. Espinosa and M. Quiros, Phys. Rev. Lett. **81** (1998) 516 [arXiv:hep-ph/9804235].
30. S. Gentile, ATL-PHYS-2004-009.
31. S. Heinemeyer, A. Nikitenko and G. Weiglein, J. Phys. Conf. Ser. **110** (2008) 072047 [arXiv:0710.3109 [hep-ph]].
32. S. Kiyoura, S. Kanemura, K. Odagiri, Y. Okada, E. Senaha, S. Yamashita and Y. Yasui, arXiv:hep-ph/0301172.
33. M. M. Muhlleitner, M. Kramer, M. Spira and P. M. Zerwas, Phys. Lett. B **508** (2001) 311 [arXiv:hep-ph/0101083].
34. M. Krawczyk, arXiv:0807.2050 [hep-ph].
35. S. Y. Choi, D. J. Miller, M. M. Muhlleitner and P. M. Zerwas, Phys. Lett. B **553**, 61 (2003) [arXiv:hep-ph/0210077].
36. C. P. Buszello, I. Fleck, P. Marquard and J. J. van der Bij, Eur. Phys. J. C **32** (2004) 209 [arXiv:hep-ph/0212396].
37. M. Duhrssen, S. Heinemeyer, H. Logan, D. Rainwater, G. Weiglein and D. Zeppenfeld, Phys. Rev. D **70** (2004) 113009 [arXiv:hep-ph/0406323].
38. A. Djouadi, H. E. Haber and P. M. Zerwas, Phys. Lett. B **375** (1996) 203 [arXiv:hep-ph/9602234].
39. GLC project: Linear Collider for TeV physics, KEK-REPORT-2003-7.
40. S. Heinemeyer, W. Hollik and G. Weiglein, Phys. Rept. **425** (2006) 265 [arXiv:hep-ph/0412214].
41. For a review of the general MSSM, see, e.g., D. J. H. Chung, L. L. Everett, G. L. Kane, S. F. King, J. D. Lykken and L. T. Wang, Phys. Rept. **407** (2005) 1 [arXiv:hep-ph/0312378].
42. E. Accomando *et al.*, arXiv:hep-ph/0608079.
43. T. Ibrahim and P. Nath, arXiv:0705.2008 [hep-ph].
44. S. Kraml, arXiv:0710.5117 [hep-ph].
45. S. Schael *et al.* [ALEPH Collaboration], Eur. Phys. J. C **47** (2006) 547 [arXiv:hep-ex/0602042].
46. S. Y. Choi, J. Kalinowski, Y. Liao and P. M. Zerwas, Eur. Phys. J. C **40** (2005) 555 [arXiv:hep-ph/0407347].
47. M. S. Carena, J. R. Ellis, A. Pilaftsis and C. E. M. Wagner, Nucl. Phys. B **625** (2002) 345 [arXiv:hep-ph/0111245].
48. D. J. Miller, R. Nevzorov and P. M. Zerwas, Nucl. Phys. B **681** (2004) 3 [arXiv:hep-ph/0304049].

49. U. Ellwanger, J. F. Gunion and C. Hugonie, *JHEP* **0502** (2005) 066 [arXiv:hep-ph/0406215].
50. R. Dermisek and J. F. Gunion, *Phys. Rev. Lett.* **95** (2005) 041801 [arXiv:hep-ph/0502105]; U. Ellwanger, J. F. Gunion and C. Hugonie, *JHEP* **0507** (2005) 041 [arXiv:hep-ph/0503203].
51. V. Barger, P. Langacker, H. S. Lee and G. Shaughnessy, *Phys. Rev. D* **73** (2006) 115010 [arXiv:hep-ph/0603247].
52. S. Y. Choi, H. E. Haber, J. Kalinowski and P. M. Zerwas, *Nucl. Phys. B* **778** (2007) 85 [arXiv:hep-ph/0612218].
53. S. F. King, S. Moretti and R. Nevzorov, *Phys. Rev. D* **73** (2006) 035009 [arXiv:hep-ph/0510419].
54. J. R. Espinosa and M. Quiros, *Phys. Lett. B* **302** (1993) 51 [arXiv:hep-ph/9212305]; G. L. Kane, C. F. Kolda and J. D. Wells, *Phys. Rev. Lett.* **70** (1993) 2686 [arXiv:hep-ph/9210242].
55. J. i. Kamoshita, Y. Okada and M. Tanaka, *Phys. Lett. B* **328**, 67 (1994) [arXiv:hep-ph/9402278].
56. K. Inoue, A. Kakuto, H. Komatsu and S. Takeshita, *Prog. Theor. Phys.* **68** (1982) 927 [Erratum-ibid. **70** (1983) 330]; **71** (1984) 413.
57. L. E. Ibanez and G. G. Ross, *Phys. Lett. B* **110** (1982) 215.
58. L. E. Ibanez, *Phys. Lett. B* **118** (1982) 73.
59. J. R. Ellis, D. V. Nanopoulos and K. Tamvakis, *Phys. Lett. B* **121** (1983) 123.
60. L. Alvarez-Gaume, J. Polchinski and M. B. Wise, *Nucl. Phys. B* **221** (1983) 495.
61. B. K. Gjelsten, D. J. Miller and P. Osland, *JHEP* **0412** (2004) 003 [arXiv:hep-ph/0410303]; *JHEP* **0506** (2005) 015 [arXiv:hep-ph/0501033].
62. H. U. Martyn, arXiv:hep-ph/0302024.
63. J. L. Feng and M. E. Peskin, *Phys. Rev. D* **64** (2001) 115002 [arXiv:hep-ph/0105100].
64. A. Freitas, A. von Manteuffel and P. M. Zerwas, *Eur. Phys. J. C* **34** (2004) 487 [arXiv:hep-ph/0310182]; *Eur. Phys. J. C* **40** (2005) 435 [arXiv:hep-ph/0408341].
65. A. J. Barr, *Phys. Lett. B* **596** (2004) 205 [arXiv:hep-ph/0405052].
66. A. Datta, K. Kong and K. T. Matchev, *Phys. Rev. D* **72** (2005) 096006 [Erratum-ibid. **72** (2005) 119901] [arXiv:hep-ph/0509246].
67. C. Athanasiou, C. G. Lester, J. M. Smillie and B. R. Webber, *JHEP* **0608** (2006) 055 [arXiv:hep-ph/0605286]; arXiv:hep-ph/0606212.
68. M. Battaglia, A. Datta, A. De Roeck, K. Kong and K. T. Matchev, *JHEP* **0507** (2005) 033 [arXiv:hep-ph/0502041].
69. S. Y. Choi, K. Hagiwara, H. U. Martyn, K. Mawatari and P. M. Zerwas, *Eur. Phys. J. C* **51** (2007) 753 [arXiv:hep-ph/0612301].
70. M. R. Buckley, H. Murayama, W. Klemm and V. Rentala, *Phys. Rev. D* **78** (2008) 014028 [arXiv:0711.0364 [hep-ph]].
71. S. Y. Choi, A. Djouadi, H. S. Song and P. M. Zerwas, *Eur. Phys. J. C* **8** (1999) 669 [arXiv:hep-ph/9812236].
72. S. Y. Choi, A. Djouadi, M. Guchait, J. Kalinowski, H. S. Song and P. M. Zerwas, *Eur. Phys. J. C* **14** (2000) 535 [arXiv:hep-ph/0002033].
73. K. Desch, J. Kalinowski, G. A. Moortgat-Pick, M. M. Nojiri and G. Polesello, *JHEP* **0402** (2004) 035 [arXiv:hep-ph/0312069].
74. S. Y. Choi, J. Kalinowski, G. A. Moortgat-Pick and P. M. Zerwas, *Eur. Phys. J. C* **22** (2001) 563 [Addendum-ibid. **C 23** (2002) 769] [arXiv:hep-ph/0108117].
75. M. M. Nojiri, K. Fujii and T. Tsukamoto, *Phys. Rev. D* **54** (1996) 6756 [arXiv:hep-ph/9606370].
76. E. Boos, H. U. Martyn, G. A. Moortgat-Pick, M. Sachwitz, A. Sherstnev and P. M. Zerwas, *Eur. Phys. J. C* **30** (2003) 395 [arXiv:hep-ph/0303110].
77. A. Bartl, H. Eberl, S. Kraml, W. Majerotto, W. Porod and A. Sopczak, *Z. Phys. C* **76** (1997) 549 [arXiv:hep-ph/9701336].
78. A. Finch, H. Nowak and A. Sopczak, arXiv:hep-ph/0211140.
79. A. Freitas and P. Z. Skands, *JHEP* **0609** (2006) 043 [arXiv:hep-ph/0606121].
80. A. Freitas, P. Z. Skands, M. Spira and P. M. Zerwas, *JHEP* **0707** (2007) 025 [arXiv:hep-ph/0703160].
81. A. Brandenburg, M. Maniatis, M. M. Weber and P. M. Zerwas, arXiv:0806.3875 [hep-ph].
82. K. Benakli and C. Moura, *in* M. M. Nojiri *et al.*, arXiv:0802.3672 [hep-ph].
83. R. M. Barnett, J. F. Gunion and H. E. Haber, *Phys. Lett. B* **315** (1993) 349 [arXiv:hep-ph/9306204]; S. Kraml and A. R. Raklev, *Phys. Rev. D* **73** (2006) 075002 [arXiv:hep-ph/0512284]; A. Alves, O. Eboli and T. Plehn, *Phys. Rev. D* **74** (2006) 095010 [arXiv:hep-ph/0605067].
84. S. Y. Choi, M. Drees, A. Freitas and P. M. Zerwas, arXiv:0808.2410 [hep-ph].
85. W. Y. Keung and L. Littenberg, *Phys. Rev. D* **28** (1983) 1067.
86. J. A. Aguilar-Saavedra and A. M. Teixeira, *Nucl. Phys. B* **675** (2003) 70 [arXiv:hep-ph/0307001].
87. N. Arkani-Hamed and S. Dimopoulos, *JHEP* **0506** (2005) 073 [arXiv:hep-th/0405159]; G. F. Giudice and A. Romanino, *Nucl. Phys. B* **699** (2004) 65 [Erratum-ibid. **B 706** (2005) 65] [arXiv:hep-ph/0406088]; N. Arkani-Hamed, S. Dimopoulos, G. F. Giudice and A. Romanino, *Nucl. Phys. B* **709** (2005) 3 [arXiv:hep-ph/0409232].
88. W. Kilian, T. Plehn, P. Richardson and E. Schmidt, *Eur. Phys. J. C* **39** (2005) 229 [arXiv:hep-ph/0408088].
89. G. A. Blair, W. Porod and P. M. Zerwas, *Eur. Phys. J. C* **27** (2003) 263 [arXiv:hep-ph/0210058].
90. S. Raby, arXiv:0710.2891 [hep-ph].
91. B. C. Allanach, arXiv:0805.2088 [hep-ph].
92. R. Lafaye, T. Plehn and D. Zerwas, arXiv:hep-ph/0404282.
93. P. Bechtel, K. Desch and P. Wienemann, *Comput. Phys. Commun.* **174** (2006) 47 [arXiv:hep-ph/0412012].
94. P. Bechtel, K. Desch, W. Porod and P. Wienemann, *Eur. Phys. J. C* **46** (2006) 533 [arXiv:hep-ph/0511006].
95. R. Lafaye, T. Plehn, M. Rauch and D. Zerwas, arXiv:0709.3985 [hep-ph]; M. Rauch, R. Lafaye, T. Plehn and D. Zerwas, arXiv:0710.2822 [hep-ph].
96. A. Freitas, W. Porod and P. M. Zerwas, *Phys. Rev. D* **72** (2005) 115002 [arXiv:hep-ph/0509056].
97. F. Depisch, A. Freitas, W. Porod and P. M. Zerwas, *Phys. Rev. D* **77** (2008) 075009 [arXiv:0712.0361 [hep-ph]].

98. R. Barbier *et al.*, Phys. Rept. **420** (2005) 1 [arXiv:hep-ph/0406039].
99. G. W. S. Hou, arXiv:0710.5424 [hep-ex].
100. U. Ellwanger, M. Rausch de Traubenberg and C. A. Savoy, Phys. Lett. B **315** (1993) 331 [arXiv:hep-ph/9307322].
101. S. Y. Choi, D. J. Miller and P. M. Zerwas, Nucl. Phys. B **711** (2005) 83 [arXiv:hep-ph/0407209].
102. J. L. Feng, *In the Proceedings of 2005 International Linear Collider Workshop (LCWS 2005), Stanford, California, 18-22 Mar 2005, pp 0013* [arXiv:hep-ph/0509309]; Class. Quant. Grav. **25** (2008) 114003 [arXiv:0801.1334 [gr-qc]].
103. F. D. Steffen, arXiv:0711.1240 [hep-ph].
104. J. R. Ellis, K. A. Olive, Y. Santoso and V. C. Spanos, Phys. Lett. B **565** (2003) 176 [arXiv:hep-ph/0303043].
105. E. A. Baltz, M. Battaglia, M. E. Peskin and T. Wizansky, Phys. Rev. D **74** (2006) 103521 [arXiv:hep-ph/0602187].
106. H. Pagels and J. R. Primack, Phys. Rev. Lett. **48** (1982) 223.
107. M. Y. Khlopov and A. D. Linde, Phys. Lett. B **138** (1984) 265.
108. J. R. Ellis, J. E. Kim and D. V. Nanopoulos, Phys. Lett. B **145** (1984) 181.
109. M. Bolz, W. Buchmuller and M. Plumacher, Phys. Lett. B **443** (1998) 209 [arXiv:hep-ph/9809381].
110. W. Buchmuller, K. Hamaguchi, M. Ratz and T. Yanagida, arXiv:hep-ph/0403203.
111. J. L. Feng, S. Su and F. Takayama, Phys. Rev. D **70** (2004) 075019 [arXiv:hep-ph/0404231].
112. K. Hamaguchi, M. M. Nojiri and A. de Roeck, JHEP **0703** (2007) 046 [arXiv:hep-ph/0612060].
113. H. U. Martyn, arXiv:0709.1030 [hep-ph]; Eur. Phys. J. C **48** (2006) 15 [arXiv:hep-ph/0605257].
114. M. Fukugita and T. Yanagida, Phys. Lett. B **174** (1986) 45.
115. W. Buchmuller, P. Di Bari and M. Plumacher, Annals Phys. **315**, 305 (2005) [arXiv:hep-ph/0401240]; Nucl. Phys. B **665**, 445 (2003) [arXiv:hep-ph/0302092].
116. M. S. Carena, M. Quiros and C. E. M. Wagner, Phys. Lett. B **380** (1996) 81 [arXiv:hep-ph/9603420].
117. M. S. Carena, A. Finch, A. Freitas, C. Milstene, H. Nowak and A. Sopczak, Phys. Rev. D **72**, 115008 (2005) [arXiv:hep-ph/0508152].
118. A. Sopczak, A. Freitas, C. Milstene and M. Schmitt, arXiv:0712.4210 [hep-ph]; A. Freitas, C. Milstene, M. Schmitt and A. Sopczak, arXiv:0712.4010 [hep-ph].